



© DIGITAL STOCK

Modeling and Simulation of Terahertz Devices

Stephen M. Goodnick and Marco Saraniti

Research and development in the exploitation of millimeter and submillimeter waves has undergone impressive growth during the last decade due to the potential technological uses of the terahertz (THz) portion of the spectrum with its unique location between the microwave (i.e., electronic) and the optical domains, which nominally corresponds to the frequency range from 300 GHz (submillimeter wave) to 10 THz. There are a number of important applications in the THz band, including atmospheric science, biodetection and imaging, THz spectroscopy, threat detection, broadband communications, and the detection of bioagents relevant to battlefield defense. Due to the sensitivity of THz

radiation to the configuration of large organic molecules, THz spectroscopy will support and sustain new technologies for the remote detection of potentially harmful bioagents [1], [2]. Furthermore, the possibility to fabricate solid-state sources and detectors will allow the production of fully integrated biosensors [3]. Wireless communication is another promising application of THz technology. In particular, mobile videophones and high-speed mobile Internet access would be greatly facilitated if THz carriers would be used at least in some links of the cellular network. All solid-state THz communication systems can be envisioned [4] that supply a valid alternative to the expensive and less-developed all-optical communication technology.

Stephen Goodnick (stephen.goodnick@asu.edu) and Marco Saraniti are with the School of Electrical, Computer, and Energy, Arizona State University, Tempe, Arizona 85287-8806 USA.

Digital Object Identifier 10.1109/MMM.2012.2216098
Date of publication: 14 November 2012

The challenge to date in making effective use of the THz portion of the spectrum is the lack of devices that operate effectively in this regime, which has historically been too high-frequency for electronic devices, and too low-frequency for photonic devices. This THz gap is being closed from both sides with the advent of electronic devices capable of operation at frequencies above 1 THz, while long wavelength photonic devices such as quantum-cascade lasers (QCLs) are closing the gap from the high-frequency side. This convergence of technologies is leading to a heretofore unknown coexistence of electronic and photonic devices operating within the same frequency range, with the potential for many new and novel hybrid electronic-photonic devices.

One of the drivers enabling closing the THz gap is nanotechnology through bandgap engineering of photonic devices like QCLs using precisely grown multiquantum confined structures to achieve ultralong wavelength operation even at room temperature. On the electronics side, the frequency response of devices such as high-electron mobility transistors (HEMTs) and heterojunction bipolar transistors (HBTs) is ultimately limited by the carrier transit time across the active device region, which decreases with decreasing dimensions (along with parasitic capacitances). In particular, for HEMTs, the ability to fabricate nanometer-scale gate-length devices while simultaneously reducing other parasitics has led to THz frequency performance.

One of the current challenges is how to accurately model the performance of such new emerging technologies. Due to the nanoscale dimensions, modeling of THz device technologies requires a more sophisticated physical representation, while high frequencies necessitate time-domain techniques capable of coupling the ultrafast carrier dynamics with external circuit components.

Semiconductor Terahertz Devices

There are a number of techniques for producing THz radiation in optoelectronic devices, e.g., electro-optic sampling through down-conversion of an optical frequency laser pulse [5]. One of the main difficulties in the direct generation of THz radiation via photonic approaches is the small semiconductor band-gap required (on the order of 1,000th of an electron volt) and lack of suitable materials with such small gaps. The QCL has been the most successful approach in meeting this challenge through radiative intersubband transitions between quantum confined states (subbands) in reduced dimensional structures such as semiconductor quantum wells and superlattices [6]. The first THz QCL devices were realized in 2001 [7]–[9] using various schemes to depopulate the lower level, such as the chirped superlattice (CSL), bound to continuum (BTC), and resonant-phonon (RP) approaches.

A summary of results by various groups was recently reviewed [10]. At present, due to the limitations of thermal broadening for such small intersubband energies, performance is limited to cryogenic temperatures and often pulsed-mode operation to reach higher temperatures. Research continues to realize full-room-temperature operation under continuous wave (CW) operation.

To close the THz gap from the electronic side, there are several solid state technologies currently capable of submillimeter wave performance, which include upconversion approaches, heterojunction bipolar transistors (HBTs) and HEMTs.

HBTs have played a central role in high-frequency electronics since their first realization using GaAs/AlGaAs heterojunctions [11]. A typical HBT structure consists of a wide bandgap semiconductor emitter, a narrower gap heavily doped base material, and either the same material for the collector [single HBT (SHBT)] or a wider bandgap collector [double HBT (DHBT)]. The wide bandgap emitter strongly suppresses minority carrier injection in the base-emitter junction, allowing in turn the use of a narrow (<50 nm), heavily doped base, which in turn reduces the base transit time and base resistance. Use of III-V materials with high-saturated velocity, e.g., InP and InGaAs, improves both the base and collector transit times. One figure of merit for high-frequency transistor performance is the short-circuit unity gain frequency (cutoff frequency), f_T , which benefits from reduced transit time in both the base and collector, while reduction of the base resistance improves the maximum frequency of oscillation, f_{max} , along with the improvement in f_T . Based on transit time considerations alone, THz operation is expected; however, reduction of other parasitics through aggressive lateral scaling of the base and collector dimensions are necessary to achieve high-frequency operation [12]. Recent results on InP/InGaAs/InP DHBT structures have demonstrated f_{max} higher than 800 GHz and $f_T = 360$ GHz [13]. Submillimeter wave InP HBT oscillators [14] and amplifiers [15], [16] have been demonstrated with operating frequencies up to 340 GHz.

Si/SiGe HBTs have recently emerged as candidates for THz HBT performance approaching the high-frequency performance of InP based devices [17], [18]. In this material system, the narrower gap SiGe is used as the base material, while Si serves as the wide bandgap material in the emitter and collector. While transport quantities such as the low-field mobility and saturated velocity are inferior to the InP system, Si technology benefits from a much more mature process technology, which allows aggressive scaling of lateral dimensions to minimize parasitic capacitances and resistances, resulting in high-performance devices. Room temperature f_T and f_{max} of 309 GHz and 343 GHz have been reported [18] with even better performance reported at cryogenic temperatures.

The HEMT [19], [20] has emerged in recent years as a preferred device for high-frequency and low-noise applications [21]. HEMTs have been made from a great variety of materials, and the efficacy of molecular-beam epitaxy has allowed strained layers to be incorporated in pseudomorphic HEMTs (*p*-HEMTs) [22]. Recently, the use of In-rich InGaAs in InP-based strained *p*-HEMTs has led to good performance in submillimeter wave amplifiers above 200 GHz [23]. Cutoff frequencies, f_T , as high as 610 GHz have been reported for this technology [24]. Of more relevance for circuit design, maximum frequency of oscillation values, f_{max} , on the order of 1.3 THz have been recently reported [25], the first field effect transistor to break the THz barrier. These devices have sub-35-nm gate lengths, hence they are nanoelectronic devices. Transconductances in excess of 2,600 mS/mm were measured in this technology, which is commensurate with the high-frequency performance. The use of In-rich InGaAs on InP-based *p*-HEMTs allows submillimeter-wave amplifiers to operate above 340 GHz [26]. A scanning electron micrograph and layer structure of an InAs based THz HEMT device is shown in Figure 1 [27]. A highly doped InGaAs cap layer is typically employed to facilitate contacting to the source and drain, and a T-gate structure is fabricated through a recessed etch to the InAlAs wide bandgap barrier material. The barrier material is delta-doped with a Si layer separated

from the $\text{In}_{.75}\text{Ga}_{.25}\text{As}$ channel, which is on the order of 20 nm thickness. This InGaAs channel can be a composite channel formed of a narrow pure InAs layer surrounded by InGaAs to decrease the effective mass as well as alloy scattering and increase mobility. An In AlAs back barrier lattice matched to a semi-insulating InP substrate helps to maintain charge confinement. THz performance is realized by decreasing the gate length below 35 nm while reducing the gate to channel barrier thickness to maintain charge control and increase the transconductance, g_m . At the same time, parasitics due to channel access resistance (due to the ungated region between the gate and source and gate and drain), contact resistance, and extrinsic resistances and capacitances must be reduced to reach THz operation.

Modeling and Simulation of Terahertz Transistor Technologies

As the technological potential of THz radiation is realized, the need for modeling and simulation tools becomes increasingly evident. New materials and devices are continually emerging as sources, detectors, and active devices in THz systems, and the parameter space for the assessment of such technologies is quite large. Modeling and simulation provide a cost-effective means of benchmarking performance and testing new ideas prior to manufacturing, as well as enabling accurate circuit design for high-frequency components. In the frequency range of interest, it becomes increasingly difficult to separate device behavior from its electromagnetic environment. New global modeling methods are required, which treat wave-device-environment interactions properly. In the following sections, we discuss physical simulation of high-frequency device structures, with a particular emphasis on InAs and GaN based HEMTs.

Full-Band Cellular Monte Carlo Device Simulation

Simulation of nanoscale devices is complicated due to the existence of ballistic, coherent transport where the wave-like behavior of particles is evident, with random, scattering events that lead to diffusive transport and a semiclassical picture of charge transport as described by the semiclassical Boltzmann transport equation (BTE). Full quantum mechanical descriptions of charge transport in HEMT and other field-effect structures have employed the nonequilibrium Greens function (NEGF) method [28]. While the formalism is quite general, in practice it has been difficult to incorporate inelastic scattering due to phonons on the same level of sophistication. Recent simulation results of Si nanowire transistors within the NEGF approach have attempted to incorporate scattering within this quantum mechanical picture [29]. Another problem with full quantum mechanical device simulation based on NEGF and other methods is that they are not typically formulated explicitly in the

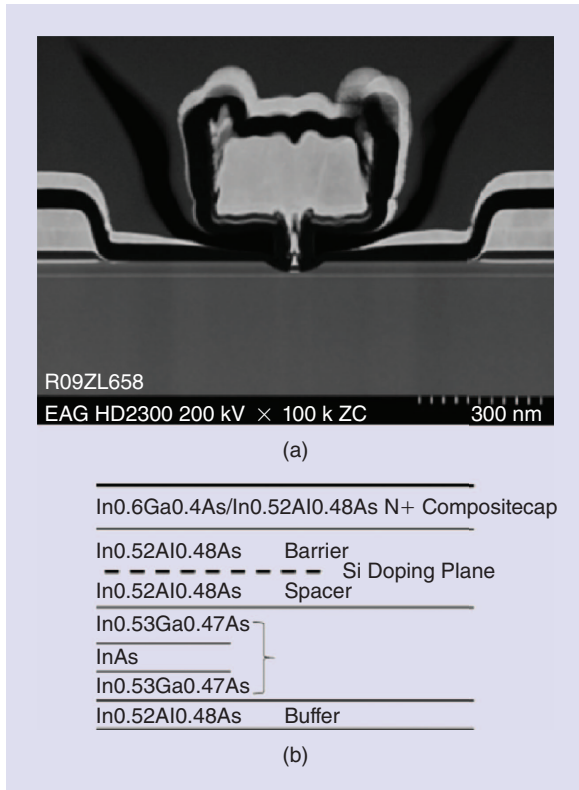


Figure 1. (a) Scanning electron micrograph (SEM) image of a 30-nm InAs HEMT on InP. (b) Layer structure of the composite channel device (from [27]).

time domain, which limits their direct applicability to modeling time-dependent and high-frequency behavior.

Particle simulation based on the ensemble Monte-Carlo (EMC) method has been used for over 30 years as a numerical method to simulate nonequilibrium transport in semiconductor materials and devices [30]. In its application to semiconductor transport problems, a random walk is generated for each particle of the ensemble, consisting of free flights under the influence of local forces acting on the particle, terminated by instantaneous, random scattering events due to scattering processes such as phonons, impurities, etc. This stochastic simulation algorithm has been shown to be equivalent to an exact solution of the semiclassical BTE and therefore fully accounts for nonstationary effects that are important for short channel devices when coupled with the appropriate set of field equations (e.g., Poisson's equation). Many body interactions beyond the simple one-electron BTE may be incorporated through, e.g., molecular dynamics treatment of the particle-particle interaction. Quantum effects are being increasingly incorporated into the technique, including phenomena such as tunneling, quantization of motion due to reduced dimensionality, effective or quantum potentials, collision broadening, finite collision duration effects, and even full quantum Monte Carlo algorithms [30]. In recent years, fullband Monte Carlo has been increasingly used [31], [32], where the full electronic bandstructure is used to describe transport and scattering. The fullband cellular Monte Carlo (CMC) method was developed to alleviate the computational burden of fullband particle-based simulation without imposing severe physical approximations [33]. The CMC approach pretabulates the transition probabilities between all initial and final states in the first Brillouin zone (BZ) of the material. This approach greatly simplifies the final state selection of the conventional fullband EMC algorithm, which usually involves a computationally intensive search

for final states in the complicated bandstructure of the material. The transition rates themselves are calculated via time dependent perturbation theory for all the relevant phonon modes in the system, which are also calculated explicitly using semiempirical methods (e.g., valence shell model) in the first BZ of the crystal. Scattering due to other elastic processes like ionized impurity, surface roughness, etc., are included as well.

In order to simulate semiconductor device behavior, the CMC transport kernel is typically coupled to a two-dimensional (2-D)/three-dimensional (3-D) multigrid Poisson solver [34], which allows a faster simulation of different families of semiconductor devices with complex geometries and boundary conditions (e.g., injecting contacts, Schottky barriers, dielectric interfaces, etc.). Typically, the coupled CMC/field solver runs on single processor machines with adequate memory to store the entire scattering look-up table, which requires 4 G of RAM or more. Due to the computational efficiency of the CMC algorithm, typical run times for an entire I-V curve are on the order of several hours, rather than days.

While the CMC algorithm is a time-domain method, solving Poisson's equation is equivalent to assuming quasi-static conditions with regard to the electromagnetic fields, which may not be valid at THz frequencies. More properly, full-wave numerical techniques such as the finite-difference time domain (FDTD) method [35] should be coupled to the transport kernel, as part of the general framework of global modeling [36].

Simulation of InAs and GaN Based HEMTs

To model the HEMT devices such as the example shown in Figure 1 using the CMC method, a non-uniform, rectangular mesh is first defined over the device domain on which Poisson's equation is repeatedly solved. Contact to the source and drain is actually quite complicated, involving tunneling into the cap layer and then tunneling through the barrier into the channel. Various models may be used to represent

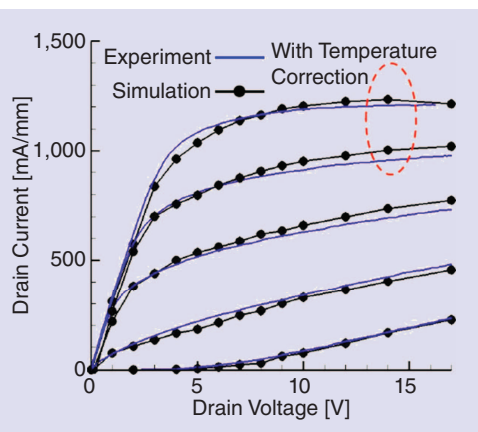
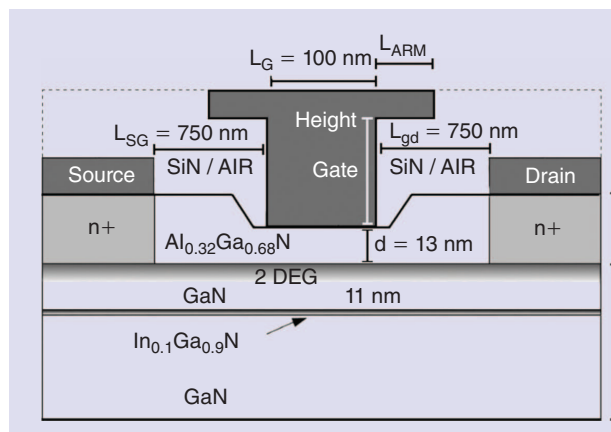


Figure 2. Cross section of a GaN HEMT simulated using the CMC method and the simulated $I_{ds} - V_g$ compared with experimental results of [37].

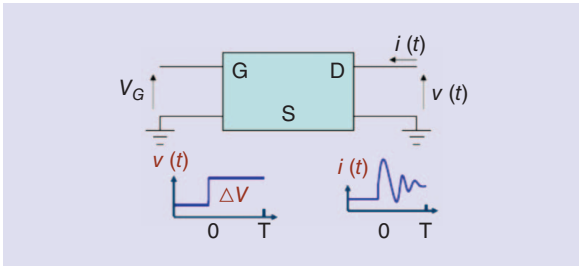


Figure 3. Schematic of the simulation of the two-port frequency response using pulse excitation.

the ohmic contacts, for example, extending the contact down to the channel, where carriers are injected or extracted in order to maintain charge neutrality on the contact, and then adding an external series resistance to account for the specific contact resistance. A Schottky contact is assumed for the gate, with a barrier height taken from experiment.

Figure 2 shows an example of a simulation of a 100-nm gate length GaN/AlGaN HEMT device structure compared with the experimental current-voltage characteristics of the same structure reported by Palacios et al. [37], which includes a thin InGaN layer as a back barrier. Good agreement with the dc current voltage characteristics is obtained, as shown in Figure 2, when the I-V curves are corrected for self-heating effects through an effective temperature rise due to Joule heating.

After obtaining agreement with dc characteristics, the next step is to perform ac transient simulation and extract high-frequency quantities of interest such as scattering parameters, cutoff frequency, etc. For transient simulation, the two-port configuration, shown in Figure 3, in which a sinusoid, a small step, or a pulse is used to excite the input (gate-source) port, and the transient current and voltage are captured at the output. Single-frequency (or multiple-tone) excitation is the most exact but computationally expensive way to characterize the frequency response, as it requires a

separate simulation for each frequency. More typically, we apply a step or pulse input and use the Fourier decomposition method [38] on the output from which the Y -parameters may be extracted for calculation of quantities of interest such as the cutoff frequency and unity power gain frequency. Care has to be taken in extracting Y -parameters from the Fourier transform of the output as the particle currents from EMC simulation are noisy due to the statistical nature of the method. For that reason, calibration of the results from pulse simulation are performed with monotone sinusoidal excitation to ensure they give the same result.

Figure 4 shows the typical result of pulse frequency analysis of one figure of merit, the short-circuit current gain, h_{21} . Figure 4(a) shows the experimental data for the device structure shown earlier in Figure 2, while Figure 4(b) is the simulated short-circuit current gain using the CMC method. Although external parasitics were not included in this set of simulations, the agreement is quite good in terms of the overall gain versus frequency and the extrapolated unity gain frequency, which suggests that extrinsic resistances and capacitances have a minimal effect in this particular set of measurements. At low frequencies, the CMC result rolls off rather than continuing to increase at 20 db/decade, which is an artifact of the finite time interval over which the simulation is run, leading to inaccurate results at frequencies below $1/t_{\text{sim}}$, where t_{sim} is the total simulation time.

Using the above approach, we have previously investigated InAs HEMTs to understand the limits of frequency response [40]. It is of interest to understand the ultimate high-frequency performance limits with scaling, and so Figure 5 shows simulation results for a hypothetical short, 300 nm source to drain InP p -HEMT for various physical (as drawn) gate lengths from 50 nm down to 10 nm [41]. Figure 5(a) shows the simulated channel velocity as a function of position relative to the physical gate (shown on the top of the graph for various gate lengths).

As seen, the peak channel velocity is much higher than peak steady-state velocity for InAs ($\sim 3 \times 10^5$ m/s) due to quasi-ballistic transport and velocity overshoot, which improves the transit time. Here, ballistic transport refers to transport in which no scattering occurs, where electrons accelerate without losing their velocity to collisions, leading to higher velocity than would be measured in steady state in bulk material. By defining the effective gate length as the distance over which carriers accelerate under the gate, we find that the simulated cutoff

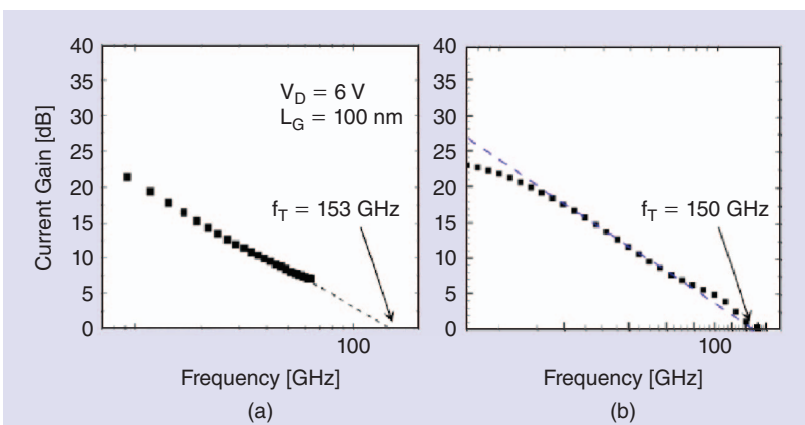


Figure 4. (a) An experimental short-circuit current gain versus frequency [37] for the device of Figure 3. (b) A simulated short-circuit current gain for the same device [39].

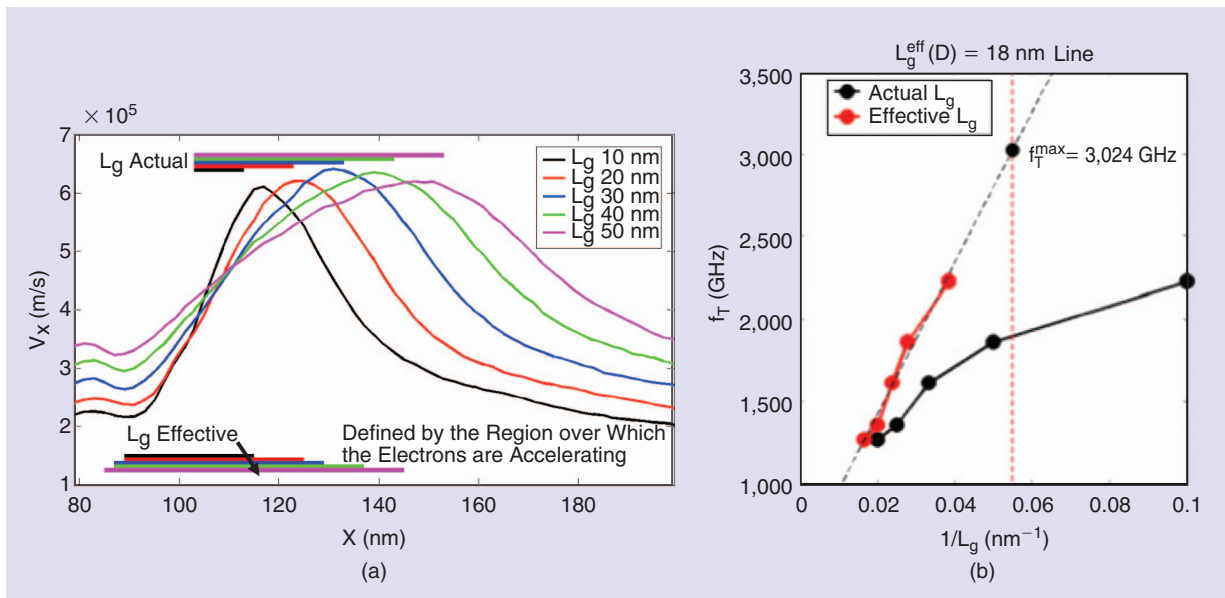


Figure 5. (a) Simulated channel velocity under the gate (top bars) for various gate lengths. The bottom bars denote the effective gate length, L_{eff} , defined as the region over which carriers accelerate. (b) Calculated f_T versus inverse gate length for both the physical and effective gate lengths and the extrapolation to zero gate length.

frequency shows good scaling with $1/L_{\text{eff}}$ as shown in Figure 5(b). This effective gate length is longer than the physical gate length due to fringing of the electric field around the physical gate and is related to the relative control of the channel by the gate. Using this metric, one sees from Figure 5(b) that multi-THz operation is potentially realizable with reduction of external parasitics with scaling into the nanometer range.

Parasitics degrade the frequency performance of transistors through resistive voltage drops and stray capacitances that introduce RC delay times associated with charging and discharging these extrinsic capacitances. One important parasitic component is that of access resistance, related to the ungated

channel region between the source and gate, and the gate and drain, in a HEMT structure. Within the standard CMC method, the effect of access resistance is easily modeled as part of the physical simulation domain. Figure 6 shows the simulated results for the GaN HEMT given in Figure 2, in which we simultaneously scale the source to gate (L_{sg}) and the gate to drain (L_{gd}) lengths for a 100 nm gate length device. The simulated cutoff frequency, f_T , is plotted as a function of both the metallurgical gate length, L_G , and the effective gate length, L_{eff} . Similar to the results shown in Figure 5(b), the cutoff frequency is a more linear function of $1/L_{\text{eff}}$ rather than the metallurgical gate length. However, the slope decreases with increasing access region length. This slope is proportional to the average transit velocity one would extract from a simple transit time analysis, and it demonstrates that the channel access resistance acts to effectively reduce the transit time across the gate, lowering the frequency response. Hence, control of the access region and its resistance is essential in realizing the full frequency response of HEMT devices.

In addition to predicting the effects of the lateral device scaling, physical device simulation may be used to look at scaling of other dimensions and their influence on performance. One parameter that strongly influences short channel device behavior is the ratio of the gate length to barrier thickness or aspect ratio, L_g/d , where d represents the thickness of the AlGaN between the gate and the GaN channel for the nitride HEMT, shown in Figure 2, or the thickness of the InAlAs barrier in the case of InAs devices. The aspect ratio is an important parameter in terms of short channel effects, as two dimensional fringing field effects become important as

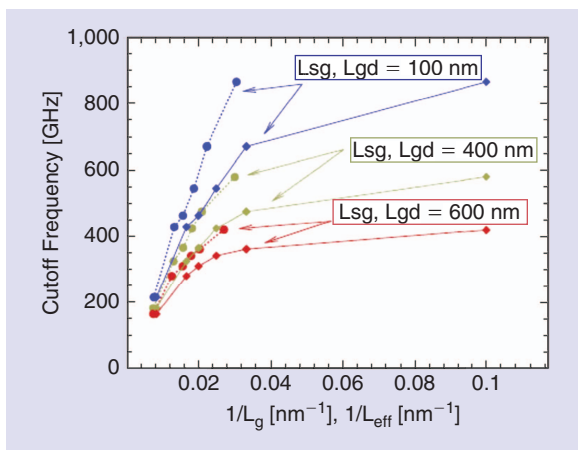


Figure 6. Cutoff frequency, f_T , plotted versus the inverse physical gate length (solid line) and the inverse effective gate length (dashed line). The devices are biased at the V_G corresponding to the peak g_m and $V_D = 5$ V [42].

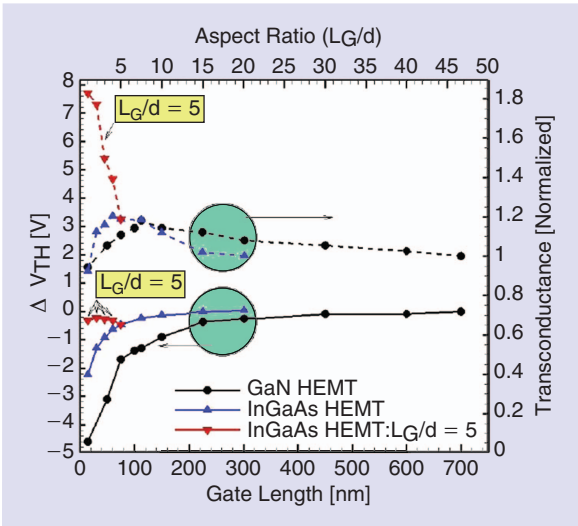


Figure 7. Comparison of dc short-channel effects for the GaN ($V_D = 10$ V) (circles) and InGaAs ($V_D = 2$ V) (triangles) HEMT devices. The device with the largest L_g/d was used as reference for V_{th} and as normalization for g_m (from [43]).

this quantity approaches unity. Figure 7 shows a study of the effect of scaling [43] on two device parameters of importance, the threshold voltage and peak transconductance, the latter being strongly correlated with the maximum frequency of operation. A comparison of two technologies is shown, GaN and InGaAs based HEMTs, using typical reported device structures such as those shown previously. If a constant barrier thickness is assumed, one can see from this figure that the threshold voltage remains constant and then decreases for a certain critical aspect ratio. This ratio is approximately 5 for the InGaAs device and 10 for the GaN device geometry considered. If one scales holding the aspect ratio,

for example in the InGaAs case to 5, it is apparent that short channel effects can be mitigated and the threshold voltage remains constant. Conversely, the transconductance, which should increase with decreasing gate length, stops increasing below the critical aspect ratio, and if the aspect ratio is preserved at 5 or above, the transconductance continues to increase as $1/L_g$. Of course, ultimately, gate leakage limits the ability of maintaining a constant aspect ratio for ultra-short channel lengths, which is also simulated using a tunneling algorithm of electrons through the gate barrier in such simulations.

Finally, one of the traditional limitations of physical device simulation is the ability to model realistic devices and circuits due to the computational limitation of the physical domain size. There has been considerable effort over the past two decades of combining physical simulation with electromagnetic or circuit simulation through so called global modeling [36]. In order to include the effects of extrinsic parasitics, as well as modeling active devices in circuits, we have coupled the full band CMC simulator to an external circuit as shown in Figure 8. Here, the CMC simulation domain encompasses the region designated as the “intrinsic simulated FET,” while the external environment is modeled as an equivalent circuit. Since the EMC device simulator is a time-domain simulation technique using a finite time step, we solve the corresponding circuit problem at each time step synchronously to simulate the full set of external voltage and current variables shown. Through this method, the effect of parasitic resistances due to the contacts, inductances due to the bias network, or parasitic capacitances due to the device layout may be included. These can be extracted by separate electromagnetic simulation of the passive structure in principal.

As an extension of this coupled device/circuit method, we have used this approach to simulate high-frequency power amplifier circuit configurations [45], [46]. Figure 9(a) shows the equivalent circuit representation of a Class B power amplifier, where the transistor is modeled using full band CMC and coupled to the external circuit as described above for Figure 8. One of the difficulties for a time-domain method such as EMC is that the typical simulation times that are practical from a computational standpoint may be orders of magnitude smaller than the RC or L/R time constants associated

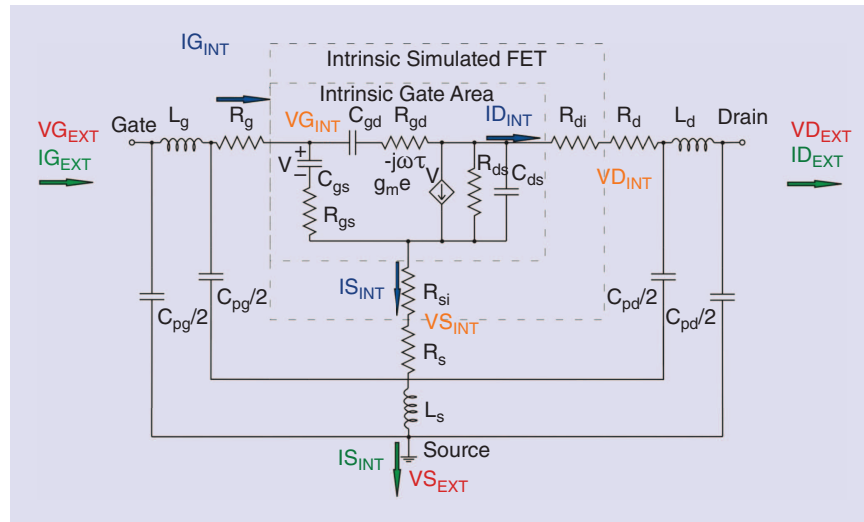


Figure 8. Equivalent circuit representation of the approach used to combine physical device simulation of the intrinsic device region coupled with an equivalent circuit representing the external parasitic components as well as bias circuit.

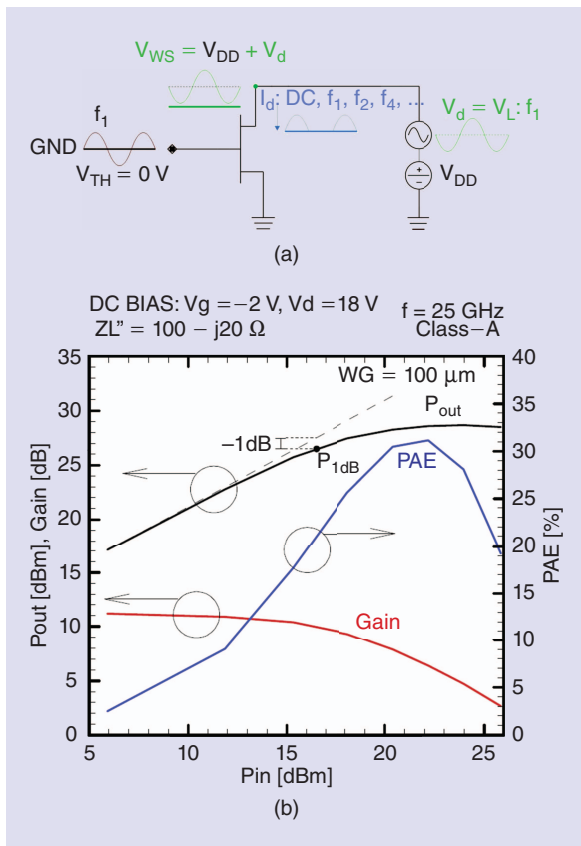


Figure 9. (a) An example of a Class-B amplifier (*i.e.*, conducting only for half of the input cycle) with high- Q matching network emulated by an active load-line technique. (b) CMC/HB simulation of a large-signal power figures of merit of the AlGaN/GaN HEMT device of Figure 2 biased as a Class-A power amplifier [44].

with the bias and coupling circuit, as well as the typical high- Q matching network used with the desired load. Hence we use an active load-line technique, which emulates the high- Q matching network with an equivalent voltage source. An iterative technique is used to match the active load to the original load with the desired impedance. A harmonic balance (HB) algorithm may be employed [44], [45] to circumvent the need for simulating the transient solution and directly obtaining steady-state response for multiple frequencies. This approach can then be used to model the performance of particular transistor technologies used in various power amplifier topologies. Figure 9(b) shows the simulated output power, gain and power added efficiency (PAE) as a function of input power for an AlGaN/GaN HEMT power amplifier operated at 25 GHz based on the transistor shown in Figure 2, which had a f_T of 150 GHz. The simulated gain and PAE compare well with measured values in similar GaN HEMT technologies and demonstrate the capability of modeling high-frequency circuits directly from first principles modeling of the physical device.

Summary

In this article, we have shown that microscopic physical simulation of transistors using full-band EMC is a powerful tool for the modeling of submillimeter wave devices and circuits. The advantage of microscopic modeling of high-frequency technologies like HEMTs and HBTs is that a complete description of the electron dynamics and device behavior is provided directly from the component materials and device structure without relying on arbitrary fit parameters. This approach provides a virtual assessment of new material and device technologies prior to actual fabrication. While EMC device simulation has traditionally been considered computationally burdensome, improved algorithms such as the CMC approach together with the rapid advances in high-performance computing in terms of speed and memory, make coupled device-circuit simulation accessible, which is of particular importance for nanometer-scale devices and high-frequency applications.

One of the challenges of approaching THz frequencies is failure of the lumped parameter representation of the external environment and circuit. Ultimately, the quasi-static assumption fails and full wave effects become important, which requires the self-consistent coupling of Maxwell's equations with the EMC device simulator. As mentioned previously, such full wave solutions were accomplished in the past through the coupling of finite difference time domain (FDTD) solutions [35] of the electromagnetic problem with the inherently time domain EMC method (see [36] and references therein) and has recently been applied, *e.g.*, to the study of high-frequency InGaAs HEMT devices [46]. The computational burden of such approaches can be quite high, due to the inherently 3-D nature of electromagnetic wave propagation, and overcoming these computational barriers is still an active area of research.

References

- [1] D. L. Woodlard, E. R. Brown, A. C. Samuels, J. O. Jensen, T. Globus, B. Gelmont, and M. Wolski, "Remote detection of bioparticles in the THz region," *IEEE MTT-S Int. Microwave Symp. Dig.*, vol. 3, pp. 1591–1594, Jun. 2002.
- [2] E. R. Brown, D. L. Woodlard, A. C. Samuels, T. Globus, and B. Gelmont, "Toward the detection of bioparticles by radar in the THz region," in *27th Int. Conf. Infrared Millim. Waves Dig.*, 2002, pp. P13–P14.
- [3] T. Baras, T. Kleine-Ostmann, and M. Koch, "Design considerations for on-chip THz analysis of biomolecules," in *Proc. 10th IEEE Int. Conf. Terahertz Electronics*, 2002, pp. 77–80.
- [4] J. W. Bowen, "Towards terahertz communication systems – System requirements," in *Terahertz Sources Systems (NATO Science Series Mathematics, Physics, and Chemistry)*, vol. 27, R.E. Miles, P. Harrison, and D. Lippard Eds. New York: Academic, 2001, pp. 269–283.
- [5] D. H. Auston, K. P. Cheung, J. A. Valdmanis, and D. A. Kleinman, "Cherenkov radiation from femtosecond optical pulses in electro-optic media," *Phys. Rev. Lett.*, vol. 53, no. 16, pp. 1555–1558, 1984.
- [6] J. Faist, F. Capasso, D. L. Sivco, C. Sirtori, A. L. Hutchinson, and A. Y. Cho, "Quantum cascade laser," *Science*, vol. 264, no. 5158, pp. 553–556, Apr. 1994.

- [7] R. Köhler, A. Tredicucci, F. Beltram, H. E. Beere, E. H. Linfield, A. G. Davies, D. A. Ritchie, R. C. Iotti, and F. Rossi, "Terahertz semiconductor-heterostructure laser," *Nature*, vol. 417, pp. 156–159, May 9, 2002.
- [8] M. Rochat, L. Ajili, H. Willenberg, J. Faist, H. Beere, G. Davies, E. Linfield, and D. Ritchie, "Low-threshold terahertz quantum-cascade lasers," *Appl. Phys. Lett.*, vol. 8, no. 18, pp. 1381–1383, 2002.
- [9] B. S. Williams, H. Callebaut, S. Kumar, Q. Hu, and J. Reno, "3.4-THz quantum cascade laser based on longitudinal-optical-phonon scattering for depopulation," *Appl. Phys. Lett.*, vol. 82, no. 7, pp. 1014–1017, 2003.
- [10] B. S. Williams, "Terahertz quantum-cascade lasers," *Nature Photon.*, vol. 1, pp. 571–525, Sep. 2007.
- [11] W. P. Dumke, J. M. Woodall, and V. L. Rideout, "GaAs-GaAlAs heterojunction transistor for high-frequency operation," *Solid-State Electron.*, vol. 15, no. 12, pp. 1339–1343, 1972.
- [12] M. J. W. Rodwell, M. Urteaga, T. Mathew, D. Scott, D. Mensa, Q. Lee, J. Guthrie, Y. Betsler, S. C. Martin, R. P. Smith, S. Jaganathan, S. Krishnan, S. I. Long, R. Pullela, B. Agarwal, U. Bhattacharyya, L. Samoska, and M. Dahlstrom, "Submicron scaling of HBTs," *IEEE Trans. Electron. Dev.*, vol. 48, no. 11, pp. 2606–2624, 2001.
- [13] E. Lobishev, Z. Griffith, V. Jain, B. J. Thibeault, M. J. W. Rodwell, D. Loubychev, A. Snyder, Y. Wu, J. M. Fastenau, and A. W. K. Liu, "200-nm InGaAs/InP type-I DHBT employing a dual-sidewall emitter process demonstrating f_{max} & G_i ; 800 GHz and $f_T = 360$ GHz," in *Proc. IEEE Int. Conf. Indium Phosphide Related Materials*, 2009, pp. 16–19.
- [14] V. Radisic, D. Sawdai, D. Scott, W. R. Deal, L. Dang, D. Li, A. Fung, L. Samoska, T. Gaier, and R. Lai, "Demonstration of a 311-GHz fundamental oscillator using InP HBT technology," *IEEE Microw. Wireless Compon. Lett.*, vol. 55, no. 11, pp. 2329–2335, Nov. 2007.
- [15] V. Radisic, D. Sawdai, D. Scott, W. R. Deal, L. Dang, D. Li, A. Cavus, A. Andy Fung, L. Samoska, R. To, T. Gaier, and R. Lai, "Demonstration of 184 and 255-GHz amplifiers using InP HBT technology," *IEEE Microw. Wireless Compon. Lett.*, vol. 18, no. 4, pp. 281–283, Apr. 2008.
- [16] J. Hacker, M. Urteaga, D. Mensa, R. Pierson, M. Jones, Z. Griffith, and M. Rodwell, "250 nm InP DHBT monolithic amplifiers with 4.8 dB gain at 324 GHz," in *IEEE MTT-S Int. Dig.*, Jun. 2008, pp. 403–406.
- [17] R. Krishivasan, Y. Lu, H. D. Cressler, J.-S. Rich, M. H. Khater, D. Ahlgren, and G. Freeman, "Half-terahertz operation of SiGe HBTs," *IEEE Electron Device Lett.*, vol. 27, no. 7, pp. 567–569, 2006.
- [18] J. Yuan, J. D. Cressler, R. Krishivasan, T. Thriivikraman, M. H. Khater, D. C. Ahlgren, A. J. Joseph, and J.-S. Rich, "On the performance limits of cryogenically operated SiGe HBTs and its relation to scaling for terahertz speeds," *IEEE Trans. Electron Device*, vol. 56, no. 5, pp. 1007–1019, 2009.
- [19] T. Mimura, S. Hiyamizu, T. Fujii, and K. Nanbu, "A new field-effect transistor with selectively doped GaAs/n-Al_xGa_{1-x}As heterojunctions," *Jpn. J. Appl. Phys.*, vol. 19, no. 5, pp. L225–L227, May 1980.
- [20] H. Daembkes, Ed., *Modulation-Doped Field Effect Transistors: Principles, Design and Technology*. New York: IEEE Press, 1991.
- [21] F. Schwierz and J. J. Liou, *Modern Microwave Transistors: Theory, Design and Performance*. Hoboken, NJ: Wiley, 2003.
- [22] R. L. Ross, S. P. Svensson, and P. Lugli, Eds., *Pseudomorphic HEMT Technology and Applications*. New York: Academic, 1996.
- [23] D. Dawson, L. Samoska, A. K. Fung, K. Lee, R. Lai, R. Grundbacher, P.-H. Liu, and R. Raja, "Beyond G-band: A 235 GHz InP MMIC amplifier," *IEEE Microw. Wireless Comp. Lett.*, vol. 15, no. 12, pp. 874–876, Dec. 2005.
- [24] S.-J. Yeon, M. Park, J. Choi, and K. Seo, "610 GHz InAlAs/In0.75GaAs metamorphic HEMTs with an ultra-short 15-nm-gate," *IEDM Tech. Dig.*, pp. 613–616, Dec. 2007.
- [25] R. Lai, X. B. Mei, W.R. Deal, W. Yoshida, Y. M. Kim, P. H. Liu, J. Lee, J. Uyeda, V. Radisic, M. Lange, T. Gaier, L. Samoska, and A. Fung, "Sub 50 nm InP HEMT device with Fmax greater than 1 THz," *IEDM Tech. Dig.*, pp. 609–612, Dec. 2007.
- [26] X. B. Mei, W. Yoshida, W. R. Deal, P. H. Liu, J. Lee, J. Uyeda, L. Dang, J. Wang, W. Liu, D. Li, M. Barsky, Y. M. Kim, M. Lange, T. P. Chin, V. Radisic, T. Gaier, A. Fung, L. Samoska, and R. Lai, "35-nm InP HEMT SMMIC amplifier with 4.4-dB gain at 308 GHz," *IEEE Electron Device Lett.*, vol. 28, no. 6, pp. 470–472, Jun. 2007.
- [27] W. Deal, X. B. Mei, K. M. K. H. Leong, V. Radisic, S. Sarkozy, and R. Lai, "THz monolithic integrated circuits using InP high electron mobility transistors," *IEEE Trans. Terahertz Sci. Technol.*, vol. 1, no. 1, pp. 25–32, Sep. 2011.
- [28] S. Datta, *Electron Transport in Mesoscopic Systems*. Cambridge, U.K.: Cambridge Univ. Press, 1997.
- [29] M. Luisier and G. Klimeck, "Atomistic full-band simulations of silicon nanowire transistors: Effects of electron-phonon scattering," *Phys. Rev. B*, vol. 80, no. 15, p. 155430, 2009.
- [30] C. Jacoboni and P. Lugli, *The Monte Carlo Method for Semiconductor Device Simulation*. Vienna, Austria: Springer-Verlag, 1989, p. 376.
- [31] K. Hess, *Monte Carlo Device Simulation: Full Band and Beyond*. Boston, MA: Kluwer, 1991, p. 310.
- [32] M. V. Fischetti and S. E. Laux, "Monte Carlo analysis of electron transport in small semiconductor devices including band-structure and space-charge effects," *Phys. Rev. B*, vol. 38, no. 14, pp. 9721–9745, Nov. 1988.
- [33] M. Saraniti and S. M. Goodnick, "Hybrid fullband cellular automaton/Monte Carlo approach for fast simulation of charge transport in semiconductors," *IEEE Trans. Electron Device*, vol. 47, no. 10, pp. 1909–1906, 2000.
- [34] M. Saraniti, A. Rein, G. Zandler, P. Vogl, and P. Lugli, "An efficient multigrid poisson solver for device simulations," *IEEE Trans. Comput.-Aided Design*, vol. 15, no. 2, pp. 141–150, Feb. 1996.
- [35] A. Taflove and S. Hagness, *Computational Electrodynamics: The Finite-Difference Time-Domain Method*, 2nd ed. Norwood, MA: Artech House, 2000, p. 852.
- [36] R. O. Grondin, S. M. El-Ghazaly, and S. M. Goodnick, "A review of global modeling of charge transport in semiconductors and full-wave electromagnetics," *IEEE Trans. Microw. Theory Tech.*, vol. 47, no. 6, pp. 817–829, 1999.
- [37] T. Palacios, A. Chakraborty, S. Heikman, S. Keller, S. P. DenBaars, and U. K. Mishra, "AlGaN/GaN high electron mobility transistors with InGaN back-barriers," *IEEE Electron Device Lett.*, vol. 27, no. 1, pp. L475–L478, Jan. 2006.
- [38] F. Schwierz and J. J. Liou, *Modern Microwave Transistors, Theory, Design and Performance*. New York: Wiley, 2003.
- [39] F. A. Marino, N. Faralli, T. Palacios, D. K. Ferry, S. M. Goodnick, and M. Saraniti, "Effects of threading dislocations on AlGaN/GaN high-electron mobility transistors," *IEEE Trans. Electron Devices*, vol. 57, no. 1, pp. 353–360, 2010.
- [40] J. S. Ayubi-Moak, D. K. Ferry, S. M. Goodnick, R. Akis, and M. Saraniti, "Simulation of ultra-submicron-gate In0.52Al0.48As/In0.75Ga0.25As/In0.52Al0.48As/InP pseudomorphic HEMTs using a full-band Monte Carlo simulator," *IEEE Trans. Electron Devices*, vol. 54, no. 9, pp. 2327–2338, 2007.
- [41] R. Akis, J. S. Ayubi-Moak, N. Faralli, D. K. Ferry, S. M. Goodnick, and M. Saraniti, "The upper limit of the cutoff frequency in ultrashort gate-length InGaAs/InAlAs HEMTs: A new definition of effective gate length," *IEEE Electron Device Lett.*, vol. 29, no. 4, pp. 306–308, 2008.
- [42] R. Soligo, D. Guerra, D. K. Ferry, S. M. Goodnick, and M. Saraniti, "Carrier dynamic study on lateral scaling and limit high-frequency performance in GaN-HEMTs," in *Proc. SISPAD*, 2012, pp. 233–236.
- [43] D. Guerra, R. Akis, F. A. Marino, D. K. Ferry, S. M. Goodnick, and M. Saraniti, "Aspect ratio impact on RF and dc performance of state-of-the-art short-channel GaN and InGaAs HEMTs," *IEEE Electron Device Lett.*, vol. 31, no. 11, pp. 1217–1219, 2010.
- [44] D. Guerra, F. A. Marino, D. K. Ferry, S. M. Goodnick, M. Saraniti, and R. Soligo, "Large-signal mm-wave InAlN/GaN HEMT power amplifier characterization through self-consistent harmonic balance/cellular Monte Carlo device simulation," in *Tech. Dig.-Int. Electron Devices Meeting*, Dec. 2011, pp. 34.2.1–34.2.4.
- [45] D. Guerra, D. K. Ferry, M. Saraniti, and S. M. Goodnick, "Millimeter-wave power amplifier circuit-device simulations through coupled harmonic balance - Monte Carlo particle-based device simulator," *Tech. Dig. Int. Microwave Symp.*, pp. 1–3, Jun. 2012.
- [46] J. S. Ayubi-Moak, R. Akis, M. Saraniti, D. K. Ferry, and S. M. Goodnick, "Physical modeling of microwave transistors using a full-band/full-wave simulation approach," in *Proc. 13th Int. Workshop Computational Electronics*, 2009, pp. 1–4.

